

Low Temperature Sintering Cu_6Sn_5 Nanoparticles for Superplastic and Super-uniform High Temperature Circuit Interconnections

Ying Zhong, Rong An, Chunqing Wang,* Zhen Zheng, Zhi-Quan Liu, Chin-Hung Liu, Cai-Fu Li, Tae Kyoung Kim, and Sungho Jin*

High temperature circuit interconnection materials are highly desirable as the power density and high temperature capabilities of present-day electronic devices are experiencing unprecedented growth due to their rapid multifunctionalization and miniaturization, especially the commercialization of wide band gap semiconductors such as silicon carbide (SiC) and gallium nitride (GaN).^[1] Although high melting point (MP) (e.g., >320 °C) solders such as Pb-, Au-, Zn-, Bi-based alloys can be utilized to provide high temperature resistance for the interconnection, they all have their own critical limitations such as toxicity, extremely high cost, poor corrosion resistance, and inferior electrical conductivity.^[2] Meanwhile, high MP alloys need higher processing temperatures to realize the melting and bonding,^[3] which may damage the circuits and substrates, especially when used in the packaging of currently burgeoning flexible and wearable devices.^[4] To address this problem, this paper proposes a novel category of circuit interconnection materials: nanoscaled intermetallics. Via nano route, Cu_6Sn_5 intermetallic nanoparticles (NPs) can act as the Holy Grail solution for the urgent hunger of high temperature bonding materials.

By taking advantage of MP suppression of NPs, nano silver (Ag) has drawn much attention as a kind of high temperature

interconnection material because of its low sintering temperature (≈ 250 °C).^[5] However, silver is still not suitable for practical applications due to its severe migration, high cost (≈ 92 times higher than Cu), long sintering time (≈ 30 min), high porosity and known toxicity for microorganism.^[6] Cu_6Sn_5 , the major intermetallic compound (IMC) in the soldering reaction between Cu substrate and liquid Sn-base solders, was mostly “hated” as the major “culprit” causing interconnection failures because of its brittle nature.^[7] However it is of low cost and abundance, exhibiting excellent coefficient of thermal expansion (CTE) match with Cu substrate, good conductivity, high mechanical stability, desirable resistance to migration and fatigue failures, and most importantly a stability of material with MP of 415 °C, which is enough for many high temperature semiconductor applications and yet not too high for fast low temperature sintering.^[8] Cu_3Sn can also be utilized as another type of Cu–Sn IMC solder with even higher stability, however, its higher MP of 676 °C means more difficult and higher temperature sintering. Such IMC solders can be useful for other applications requiring higher stability. Processing, structure and properties on Cu_3Sn based solders will be reported elsewhere in the future.

Some recent research has reported nano-sizing of Cu_6Sn_5 through methods such as ball-milling, gas-atomization, chemical reduction, etc. for possible battery electrode applications.^[9] However, the resultant Cu_6Sn_5 particle size was substantially larger than the necessary dimension to enable desirably significant reduction of the MP and associated sintering temperature.^[10] Better synthesis methods which can manipulate the size of Cu_6Sn_5 NPs at sub-10 nm scale should be developed.

According to the inverse Hall–Petch phenomenon,^[11] nanocrystalline metallic materials can be made superplastic and highly stress-accommodating, as is most desired for circuit bonding.^[12] This phenomenon offers us an exciting new avenue of eliminating the brittleness of Cu_6Sn_5 and maintaining the advantageous thermal, electrical, and mechanical properties of sintered nanoscale Cu_6Sn_5 .^[13]

In this Communication, we developed a low cost, efficient, and environmental friendly coprecipitation reduction method to tailor the size and initial sintering temperature of sub-10 nm Cu_6Sn_5 NPs. Confirmed by monitoring the consolidation of Cu_6Sn_5 NPs during in situ TEM heating,

Y. Zhong, Dr. R. An, Prof. C. Wang, Dr. Z. Zheng
State Key Laboratory of Advanced Welding and Joining
Harbin Institute of Technology
Harbin 150001, China
E-mail: wangcq@hit.edu.cn

Y. Zhong, Dr. C.-H. Liu, Dr. T. K. Kim, Prof. S. Jin
Materials Science and Engineering
University of California at San Diego
9500 Gilman Dr., La Jolla, CA 92093, USA
E-mail: jin@ucsd.edu

Dr. R. An, Prof. C. Wang
Key Laboratory of Microsystems and Microstructures Manufacturing
Ministry of Education
Harbin Institute of Technology
Harbin 150080, China

Prof. Z.-Q. Liu, Dr. C.-F. Li
Institute of Metal Research
Chinese Academy of Sciences
Shenyang 110016, China

DOI: 10.1002/sml.201500896



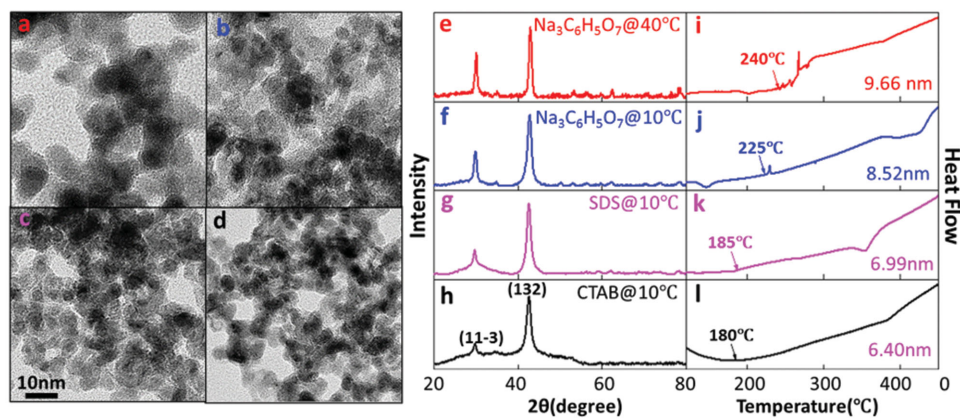


Figure 1. Influence of synthesis parameters on the morphology, XRD results and DSC results of Cu_6Sn_5 NPs. a,e,i) Sodium citrate as surfactant at 40 °C. b,f,j) Sodium citrate as surfactant at 10 °C. c,g,k) SDS as surfactant at 10 °C. d,h,l) CTAB as surfactant at 10 °C.

Cu_6Sn_5 NPs can start bonding at ≈ 180 °C, which is ≈ 235 °C lower than bulk Cu_6Sn_5 and compatible with conventional Sn-based solders. After sintering, the connections can recover the high MP of Cu_6Sn_5 (415 °C) and serve reliably for high temperature devices. More excitingly, the low temperature sintered interconnections are superplastic, overcoming the brittle nature of intermetallics as they are made of pore-free nanograins; and the interface is super-uniform according to focused ion beam (FIB) cross section. In addition, the potential of Cu_6Sn_5 for high temperature circuit interconnection was approved by its anisotropy and other relevant properties.

Synthesis of Cu_6Sn_5 NPs was based on an aqueous solution coprecipitation reduction method without using expensive organic chemicals or external heating (Figure S1a, Supporting Information). The reaction took place immediately once the CuCl_2 and SnCl_4 precursor solution was dropped into the reducing solution, making this method very time-efficient. As shown in **Figure 1**, we were able to manipulate the particle size and then the sintering temperature by carefully altering the synthesis temperature and the surfactant employed. Shown in Figure 1a–d are the synthesized NPs with sodium citrate ($\text{Na}_3\text{C}_6\text{H}_5\text{O}_7$) as surfactant at 40 °C, sodium citrate as surfactant at 10 °C, sodium dodecyl sulfate (SDS, $\text{CH}_3(\text{CH}_2)_{11}\text{OSO}_3\text{Na}$) as surfactant at 10 °C and cetyltrimonium bromide (CTAB, $(\text{C}_{16}\text{H}_{33})\text{N}(\text{CH}_3)_3\text{Br}$) as surfactant at 10 °C (see Figure S2, Supporting Information, for size distribution, HRTEM image and fast Fourier transform (FFT) result). The average particle size reduced with the decreasing of synthesis temperature and increasing of carbon chain length of the surfactant: 9.66, 8.52, 6.99, and 6.40 nm, respectively. The X-ray diffraction (XRD) peaks in Figure 1e–h matched very well with those of η' - Cu_6Sn_5 (C2/c (15), PDF card #00-045-1488), with main peaks of (1,1,-3) and (1,3,2) without any other impurities detected. Corresponding with Figure 1a–d, the peak widths in the XRD results increased slightly with the reduction of the crystal size. The differential scanning calorimetry (DSC) results shown in Figure 1i–l are very remarkable. As NPs do not have an accurate melting point like bulk materials, the temperature starting endothermic activity was defined as the initial coalescence (or sintering) temperature.^[14] When the particle size was 9.66 nm, the initial coalescence temperature can be reduced from

415 °C of bulk Cu_6Sn_5 to ≈ 240 °C. This dramatically reduced temperature was further reduced with even smaller particle sizes, and can be as low as ≈ 225 °C for 8.52 nm particles, ≈ 185 °C for 6.99 nm particles and ≈ 180 °C when the particle size was as small as 6.4 nm (thermal gravity analysis (TGA) results are shown in Figure S3, Supporting Information). This result clearly demonstrates a significant reduction in the initial sintering temperature along with the decrease of NP diameters just like other metallic materials.^[15] This exciting 235 °C reduction from 415 °C to 180 °C exceeds most reports on utilizing nanosized particles to get suppressed MPs.^[16] The extremely increased surface to volume ratio by the reduced particle size is considered the main reason for the MP reduction.^[17] Equation (1) is one of the most commonly used expressions of the initial sintering temperature as dependence on the NP size based on thermodynamic theory^[14]

$$T_{\text{is}}(r) = 0.3T_{\text{m}} \exp \left[-\frac{2S_{\text{m}}(\infty)}{3k} \frac{1}{(r/r_0) - 1} \right] \quad (1)$$

where $T_{\text{is}}(r)$ is the initial sintering temperature, T_{m} is the melting point of the bulk material, S_{m} is the bulk melting entropy, r is particle radius, $r_0 = 3h$ (where h is atomic diameter), k is Boltzmann constant. Therefore, agree with the results in Figure 1i–l, as r reduced, $T_{\text{is}}(r)$ can be lowered dramatically as demonstrated experimentally. This remarkable MP reduction provides an enabling foundation for the desired low temperature consolidation of the Cu_6Sn_5 NPs, which was also proved by our in situ TEM hot stage experiment.

The coalescence behavior of Cu_6Sn_5 NPs (CTAB as surfactant) during in situ TEM heating is shown in **Figure 2** step by step at different temperatures and dwelling times. Movie 1 in the Supporting Information describes the dynamic action taken in real time. The higher the temperature is, the faster the particles can grow; at the same temperature, the longer the dwelling time is, the bigger the NPs can grow to. Specifically, Figure 2a is the Cu_6Sn_5 NPs at 20 °C before heating. During the in situ TEM experiments, the temperature increased at 20 °C intervals, and dwell at each temperature for 3 min to observe the change of the NPs morphology. The results indicate that the temperature for the significant coalescence started from ≈ 180 °C, which matches the initial coalescence

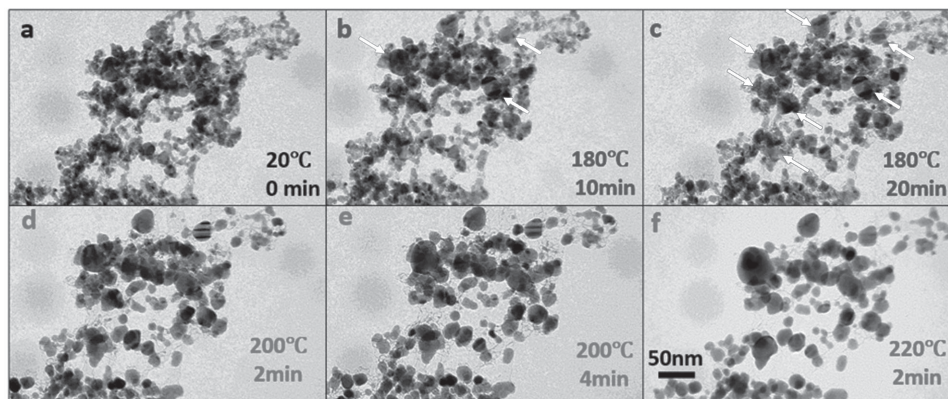


Figure 2. Consolidation behavior of Cu_6Sn_5 NPs (CTAB as surfactant) during in situ TEM heating. a) Original Cu_6Sn_5 NPs before heating with average size of ≈ 7 nm. b) After keeping at 180°C for 10 min with average size reaching ≈ 8 nm. c) After keeping at 180°C for 20 min with average size reaching ≈ 11 nm. d) After heating up to 200°C and dwelling at this temperature for 2 min. e) After dwelling at 200°C for 4 min. f) After increasing the temperature to 220°C and dwelling at this temperature for 2 min.

temperature obtained from the DSC result in Figure 11. The kinetics of nanoparticle coalescence at 180°C was quite slow, so we kept at this temperature longer. After 10 min, there was only several local regions with higher particle density as marked by arrows in Figure 2b coalesced. After 20 min at 180°C , there were some additional areas grew and consolidated as marked by the added arrows in Figure 2c, while those regions previously already coalesced continued growing. The TEM temperature was then raised to 200°C , followed by dramatically accelerated coalescence, as can be seen clearly in Figure 2d,e. The coalescence phenomenon happened almost everywhere. In 2 min time, the average particle size was increased from ≈ 11 nm (Figure 2c) to ≈ 16 nm (Figure 2d). After dwelling 4 min at 200°C , the particle size increased to ≈ 21 nm (Figure 2e). Then the temperature was increased again to 220°C , after which 2 min time, the particles started to become more rounded with the average size reaching ≈ 30 nm (Figure 2f), which is a typical premelting phenomenon as was firstly presented by Pawlow in 1909: even below its melting point, quasi-liquid films can be observed on crystalline surfaces.^[18] Atoms in the quasi-liquid film have a lower energy and are easier to diffuse, which can induce rapid coalescence of the particles. This quasi-liquid layer can benefit the sintering procedure such as two snowballs with premelted surface being able to get connected together very easily.^[19] According to thermodynamic theory, the thickness of this quasi-liquid film d varies logarithmically with temperature T as

$$d \propto \ln\left(1 - \frac{T}{T_m}\right) \quad (2)$$

where T_m is the MP of the bulk material, meaning the growth of quasi-liquid films is enhanced with an increase in the temperature T .^[19]

By ultrasonically dispersing Cu_6Sn_5 NPs into ethanol and then mixing them with dispersant and flux, we were able to prepare a convenient nano Cu_6Sn_5 paste for interconnection applications (see Figure S1b, Supporting Information). Two copper substrates were connected by sintering Cu_6Sn_5 paste

at 200°C for 20 min with a pressure of 5 MPa in vacuum (see Figure S1c, Supporting Information). (An inert gas atmosphere can also be used.) In the cross section image of the sandwich structure in Figure 3a, the sintered Cu_6Sn_5 shows a very robust interconnection between two copper substrates and there was no noticeable pores found at all. This is exciting as such a pore-free joint is highly desirable, and by comparison, most of the sintered nano Ag structures tend to exhibit high porosities. This absence of undesirable pores in consolidated Cu_6Sn_5 is believed to be due to the much lower melting point of Cu_6Sn_5 than Ag (415°C versus 962°C), Equation (2) and the premelt phenomena observed in Figure 2 can help to explain it: materials with a lower MP can have a thicker layer of melted surface than high MP materials at the identical temperature. The temperature needed for the premelt to occur is also related to the curvature of the particle κ as expressed below in Equation (3)^[19]

$$T = (1 - c\kappa)T_m \quad (3)$$

where c is a material related constant. For a certain material, the growth of the particle, meaning the reduction of κ , can lead to an increase of the temperature needed for the premelt. At a given temperature, after reaching a critical curvature or particle size, the particle growth could dramatically slow down because of the lack of the quasi-liquid film for fast diffusion. So there is a critical curvature for each temperature, meaning that there should be a temperature at which the Cu_6Sn_5 NPs stop rapid growth and remain nanocrystalline. At a temperature around 200°C , there was no quasi-liquid film observed in Ag NPs.^[20] The densification of Ag NPs is mostly dominated by solid state diffusion with a typical necking process, which is not sufficient for the desired rapid connection between adjacent particles. Ag NPs are growing with the concomitant curvature decrease, and the temperature needed for premelt becomes even higher, leading to a termination of active coalescence process before the bonding material reaches the desired dense sintered structure. By contrast, for Cu_6Sn_5 NPs with a much lower bulk MP, there is already a thick quasi-liquid film observed at about 200 – 220°C , which makes good particle connectivity easy. One then just needs to

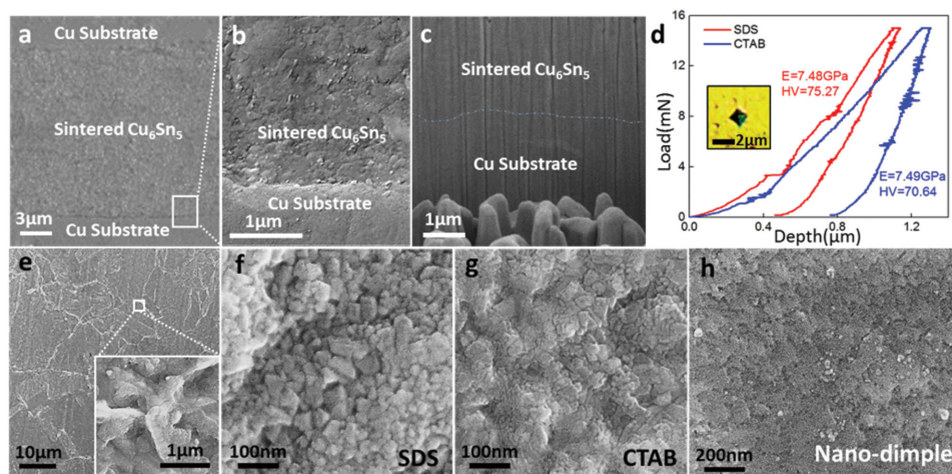


Figure 3. The result of connecting Cu substrates by sintering Cu_6Sn_5 NPs. a) The cross section showing the sound connection in the sandwich structure. b) The high magnification image of the interface between sintered Cu_6Sn_5 and Cu substrate. c) FIB result showing the super-uniform interface (dotted line is the location where the interface is supposed to be observed). d) The micro-hardness test results on cross section of sintered Cu_6Sn_5 , the insert image is the indentation by the hardness test. e) Large area sintered Cu_6Sn_5 , and the insert image is the higher magnification image showing the brighter lines are not cracks but dense sintered Cu_6Sn_5 . f) The high magnification image of the sintered Cu_6Sn_5 with SDS as surfactant showing the grain size as 25.61 nm. g) The high magnification image of the sintered Cu_6Sn_5 with CTAB as surfactant showing the grain size as 21.60 nm. h) The nano-dimple fracture surface of the sintered Cu_6Sn_5 .

wait for the radius of curvature κ to reach its critical value to halt the quick grain growth so as to obtain and maintain the nanograin.

The higher magnification image (Figure 3b) of the interface between the sintered Cu_6Sn_5 and lower Cu substrate also clearly shows a robust, pore-free interconnection. The interface got by FIB in Figure 3c is extremely exciting that there is no recognizable interface phase between sintered Cu_6Sn_5 and Cu substrate (the dotted line indicates where the interface is supposed to be observed) as they show almost the same contrast in SEM, which means the interface is super-uniform. According to the linear result of the interface in Figure S4, Supporting Information, the interface layer is Cu_3Sn with a thickness of only 200 nm as an evidence of decent joining. This super-uniform interface is highly desirable for interconnections as it can eliminate the interface mismatch which is claimed as one of the most common causes of failure.

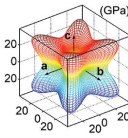
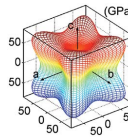
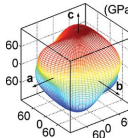
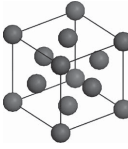
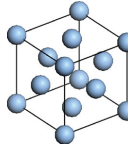
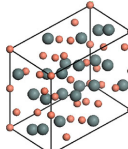
In Figure 3d, we carried out micro-hardness tests on the cross section of the samples and compared the hardness of sintered Cu_6Sn_5 regions prepared from different original particle sizes. The relative hardness value Vickers hardness (HV) of the sintered Cu_6Sn_5 (≈ 6.99 nm) with SDS as surfactant was 75.27, and the other (≈ 6.40 nm) with CTAB was just 70.64, which was only $\approx 20\%$ of bulk Cu_6Sn_5 material, indicating the ease of deformation in the bonded nano Cu_6Sn_5 material. No micro-cracking was observed near the indentation mark in the inset image in Figure 3d, also meaning the material tested was soft. The Young's modulus of the sintered nano Cu_6Sn_5 with SDS and CTAB as surfactant was just 7.48 and 7.49 GPa, respectively, both of which are only $\approx 10\%$ of the modulus of bulk Cu_6Sn_5 and only $\approx 50\%$ of Sn based solders estimated from similar micro-hardness testing.

Figure 3e demonstrates that Cu_6Sn_5 NPs can be sintered very densely without any noticeable cracks or pores in a very large area. The brighter lines as can be seen clearly in the inset

higher magnification image in Figure 3e are not cracks but densely sintered Cu_6Sn_5 . Shown in Figure 3f is the nanocrystalline structure of sintered Cu_6Sn_5 (via SDS surfactant) with an average diameter of 25.61 nm. Figure 3g represents the sintered Cu_6Sn_5 (via CTAB surfactant) with a mean grain size of 21.60 nm. Combining with the hardness and Young's modulus results, it can be proved that by maintaining the nanocrystalline structure, we can produce mechanically compliant Cu_6Sn_5 joints showing inverse Hall-Petch phenomenon:^[21] the nanocrystalline Cu_6Sn_5 gets softer as grain size is reduced below a critical value. The less the Young's modulus is, the more deformation will occur in the material under the same stress, which is desirable for absorbing stresses caused by various reasons in circuit connection and packaging, such as CTE mismatch, component distortion, thermal cycling, and so forth. Figure 3h is the nano-dimple fracture surface after pulling test, which is another strong evidence of the soft nature of Cu_6Sn_5 nanocrystalline. At the same time of overcoming the brittleness of Cu_6Sn_5 with superplastic nanograins, the high-temperature and migration resistance of bulk Cu_6Sn_5 was recovered after sintering, which is a breakthrough advancement toward the Holy Grail of reliable circuit connections for future advanced and powerful electronics.

For circuit bonding materials, thermal, electrical, and mechanical properties and even cost should be considered. **Table 1** shows some comparison between the nanocrystalline Cu_6Sn_5 joints with Pb (the main stream material in conventional high temperature soldering) and nano Ag as one of the most popular, low-temperature-sinterable, Pb-free, high temperature interconnection material. In terms of high temperature solder bonding, Pb-based solders cannot survive the high junction temperature of devices such as SiC or GaN. Nano Ag can be sintered at about 250–300 °C and recover its high MP of 962 °C. But the sintering temperature and time

Table 1. The property comparison of Pb, Ag, nano Ag, Cu₆Sn₅, and nano Cu₆Sn₅.

Interconnection materials	Pb	Ag	Nano Ag	Cu ₆ Sn ₅	Nano Cu ₆ Sn ₅
Melting point or sintering starting temperature [°C]	327	962	250–300	415	180–220
Thermal conductivity [W cm ⁻¹ K ⁻¹]	35.3	429	30–240	47.7	47.7
Electrical resistivity [mΩ cm]	20.8	1.6	2.5–21	17.5	17.5
CTE at 25 °C [×10 ⁻⁶ °C ⁻¹]	28.9	19.6	19.6	16.3	16.3
Vickers hardness	39	251	40–80	378	70–75
Measured Young's modulus [GPa]	16	83	60	119	7.5
E_{\max} [GPa]	51.4	121		152	
Orientation of E_{\max}	<1,1,1>	<1,1,1>		[-3,0,2]	
E_{\min} [GPa]	14.9	42.9		96.5	
Orientation of E_{\min}	<1,0,0>	<1,0,0>		[2,0,1]	
A [%]	55.1	47.7		22.3	
Directional dependence of Young's modulus					
Lattice structure					

for nano Ag bonding are both quite excessive as compared to those for current soldering operations, making them much more expensive and time consuming. The Cu₆Sn₅ NPs possess nearly ideal sintering temperature and time matching very well with that for most commonly used Sn-based solders, and the recovered bulk MP of the sintered Cu₆Sn₅ joint (415 °C) is sufficiently high for protecting the circuit connection bonds from electromigration and high temperature fatigue. When it comes to electrical conductivities, the high porosity in the sintered Ag often produces inconsistent and somewhat lowered conductivity values often worse than that for Pb. By contrast, sintered nano Cu₆Sn₅ material is generally pore-free, can exhibit more reliable electrical properties than Pb. Furthermore, Cu₆Sn₅ has almost the same CTE with copper substrate ($16.3 \times 10^{-6} \text{ °C}^{-1}$ for Cu₆Sn₅ versus $16.0 \times 10^{-6} \text{ °C}^{-1}$ for Cu), which can essentially eliminate the CTE mismatch problem between the solder and the substrate, especially with the super-uniform interface shown in Figure 3c.^[22] Also, by virtue of nanograin structures, the Young's modulus of nano Cu₆Sn₅ is less than half of Pb. This advantageous mechanical compliance helps to overcome the inherent brittleness of Cu₆Sn₅ and yet protects the joints from failure even at high operating temperatures. In terms of practical industrial applications, Cu₆Sn₅ is quite inexpensive (only $\approx 1/3$ of Sn, $\approx 1/50$ of Ag, and five orders of magnitude less than the price for Au80Sn20 solder) and contains no critical or rare elements.

Anisotropy also plays a significant role in mechanical properties of circuit bonding materials especially for high

operating temperatures and ultrafine pitches. Here, we define elastic anisotropy $A(\%)$ as

$$A(\%) = \frac{E_{\max} - E_{\min}}{E_{\max} + E_{\min}} \quad (4)$$

where E_{\max} and E_{\min} are the maximum and minimum Young's modulus of the material along certain crystallographic orientations.^[23] As reported before, when the temperature reaches 165 °C, the maximum shear stress at the Sn grain boundary can reach a quite high value of ≈ 82.31 MPa to cause grain separation ($E_{\max(\text{Sn})} = 69$ GPa, $E_{\min(\text{Sn})} = 22.9$ GPa, $A_{(\text{Sn})} = 50.1\%$ as can be found in Figure S5, Supporting Information).^[24] The less anisotropic the material is, the easier for all the grains to deform uniformly and simultaneously, thus less stress between grains and then less cracks during deformation.^[25] As summarized in Table 1, The anisotropy of Pb is very severe with $E_{\max(\text{Pb})}$ being 51.4 GPa at <1,1,1> orientation and $E_{\min(\text{Pb})}$ as 14.9 GPa at <1,0,0> direction, making $A_{(\text{Pb})}$ as much as 55.1% (Figure S6, Supporting Information), which explains its easily captured grain slide during tensile test.^[26] The elastic anisotropy of Ag is 47.7%, with $E_{\max(\text{Ag})}$ as 121 GPa and $E_{\min(\text{Ag})}$ as 42.9 GPa (Figure S7, Supporting Information), which reduced the crack resistance of sintered silver as irregularly distributed Ag NPs with random orientations cannot easily deform uniformly. Cu₆Sn₅ has a very low anisotropy in Young's modulus, with the $A_{(\text{Cu}_6\text{Sn}_5)}$ value being only 22.3% as $E_{\max(\text{Cu}_6\text{Sn}_5)}$ being 152 GPa at <-3,0,2> orientation and $E_{\min(\text{Cu}_6\text{Sn}_5)}$ being 96.5 GPa at <2,0,1> direction (Figure S8, Supporting Information), meaning substantially

reduced level of stress between grains with different orientations and hence reduced tendency for grain separation and better reliability at high operating temperature. This advantageous characteristics can also contribute to the higher crack resistance of the sintered Cu_6Sn_5 structure. Yet another advantage of nano Cu_6Sn_5 is that with the sub-10 nm nanoparticle paste of Cu_6Sn_5 , sub-10 nm resolution screen printing, ink-jet printing, 3D printing, as well as sub-micrometer resolution nano transfer imprinting can be possible.

To summarize, this Communication presents a novel, breakthrough approach of turning the typically unwanted, hard, and brittle Cu_6Sn_5 intermetallic compound material into a quite desirable and superior high-temperature circuit connection material with stress-accommodating properties via nano route. Sub-10 nm level nanoparticles were easily synthesized and made into a paste for easy usage. The 415 °C high-melting-temperature Cu_6Sn_5 can be bonded at a low temperature of even below ≈ 200 °C. A pore-free, nanograined, and superplastic connection with super-uniform interface was thus created after the low temperature and short time consolidation, as demonstrated by bonding experiments and actual in situ TEM observation of nanoparticle consolidation process. Such a nano Cu_6Sn_5 bonding material can be a useful and practical attachment material easy to process for assembly of Pb-free, high temperature components or flexible devices with ultrafine pitch configurations. This concept of transforming brittle intermetallics into nonbrittle, superplastic, stress-accommodating and high temperature-resistant bonding material via nano route can also be applied broadly to many other intermetallic compounds including Cu–Sn, Ni–Sn, Ag–Sn, Zn–Sn, Cu–Al to create highly reliable, circuit connection materials that can also enable ultra-high density, micrometer or sub-micrometer dimension circuit contact pads.

Experimental Section

Cu_6Sn_5 NP Synthesis: In a typical reaction, a $\text{CuCl}_2 \cdot \text{H}_2\text{O}$ and $\text{SnCl}_4 \cdot 5\text{H}_2\text{O}$ mixture in molar ratio of 6:5 (for example, 340.5 mg versus 583.0 mg) was dissolved in 20 mL deionized (DI) water together with certain amount of sodium citrate to get the “solution A” ready. For “solution B,” we first added surfactant into 50 mL DI water, and then dissolved NaBH_4 which was twice the amount of Sn^{4+} and Cu^{2+} to ensure the complete reduction. The reaction took place immediately after solution A was dropped into solution B.

Sintering: After screen printing fresh solder paste onto phosphoric acid washed (for 2 min) Cu substrates, 5 MPa pressure was added to assist the sintering process. The samples were heated up to 200 °C in vacuum for 20 min to realize dense sintering.

Characterization: Morphology and size distribution of Cu_6Sn_5 NPs were observed with JEM-2100 transmission electron microscope. With the Gatan single tilt heating holder and the smartest hot stage controller, the temperature, heating rate, and dwell time were able to control as by manipulating the current. The composition of the NPs was characterized by XRD (Bruker D2 X-ray diffractometer) with Cu $\text{K}\alpha$ radiation. The differential scanning calorimeter (DSC) and thermal gravimetric analysis (TGA) tests were carried out in Perkin-Elmer DSC 8000 thermal analyzer and

Pyris TGA, respectively, at a heating rate of 20 °C min^{-1} with a 40 mL min^{-1} flow of nitrogen. DUH-W201S ultra micro-hardness tester was used to characterize the hardness of the cross section of the sintered solder joints (test force: 200 mN). FEI Scios Dual-Beam FIB/SEM was used to get the fresh cross section.

Supporting Information

Supporting Information is available from the Wiley Online Library or from the author.

Acknowledgements

C.Q.W. and S.J. contributed equally to this work. This research was supported by National Natural Science Foundation of China under Grant No. 51374084, Iwama Endowed Fund at UC San Diego, and by grants from the Power Electronics Science and Education Development Program of Delta Environmental & Educational Foundation.

- [1] a) Y. Cui, C. M. Lieber, *Science* **2001**, *291*, 851; b) S. Kawata, H. B. Sun, T. Tanaka, K. Takada, *Nature* **2001**, *412*, 697.
- [2] C. Chen, H. Tong, K. Tu, *Annu. Rev. Mater. Res.* **2010**, *40*, 531.
- [3] T. Ishizaki, R. Watanabe, *J. Mater. Chem.* **2012**, *22*, 25198.
- [4] a) G. S. Jeong, D. H. Baek, H. C. Jung, J. H. Song, J. H. Moon, S. W. Hong, I. Y. Kim, S. H. Lee, *Nat. Commun.* **2012**, *3*, 977; b) J. Ji, Z. Zhou, X. Yang, W. Zhang, S. Sang, P. Li, *Small* **2013**, *9*, 3014.
- [5] a) C. Yang, H. Gu, W. Lin, M. M. Yuen, C. P. Wong, M. Xiong, B. Gao, *Adv. Mater.* **2011**, *23*, 3052; b) J. Perelaer, R. Jani, M. Grouchko, A. Kamysny, S. Magdassi, U. S. Schubert, *Adv. Mater.* **2012**, *24*, 3993.
- [6] a) P. Cronholm, H. L. Karlsson, J. Hedberg, T. A. Lowe, L. Winnberg, K. Elihn, I. O. Wallinder, L. Möller, *Small* **2013**, *9*, 970; b) M. Maruyama, R. Matsubayashi, H. Iwakuro, S. Isoda, T. Komatsu, *Appl. Phys. A: Mater. Sci. Process.* **2008**, *93*, 467.
- [7] M. S. Park, R. Arroyave, *Acta Mater.* **2012**, *60*, 923.
- [8] M. S. Park, S. L. Gibbons, R. Arroyave, *Acta Mater.* **2012**, *60*, 6278.
- [9] H. P. Zhao, X. M. He, C. Y. Jiang, C. R. Wan, *Science* **2006**, *18*, 1710.
- [10] a) P. Buffat, J. P. Borel, *Phys. Rev. A* **1976**, *13*, 2287; b) S. Bhanushali, P. Ghosh, A. Ganesh, W. Cheng, *Small* **2014**, *11*, 1232.
- [11] X. Li, Y. Wei, L. Lu, K. Lu, H. Gao, *Nature* **2010**, *464*, 877.
- [12] a) J. Schiøtz, F. D. Di Tolla, K. W. Jacobsen, *Nature* **1998**, *391*, 561; b) R. Longtin, E. Hack, J. Neuenschwander, J. Janczak-Rusch, *Adv. Mater.* **2011**, *23*, 5812.
- [13] J. Schiøtz, T. Vegge, F. D. Di Tolla, K. W. Jacobsen, *Phys. Rev. B* **1999**, *60*, 11971.
- [14] Z. Fang, H. Wang, *Int. Mater. Rev.* **2008**, *53*, 326.
- [15] M. José-Yacamán, C. Gutierrez-Wing, M. Miki, D. Q. Yang, K. Piyakis, E. Sacher, *J. Phys. Chem. B* **2005**, *109*, 9703.
- [16] a) P. Grammatikopoulos, C. Cassidy, V. Singh, M. Sowwan, *Sci. Rep.* **2014**, *4*, 5779; b) T. Karabacak, J. S. DeLuca, P. I. Wang, G. A. Ten Eyck, D. Ye, G. C. Wang, T. M. Lu, *J. Appl. Phys.* **2006**, *99*, 064304.
- [17] C. T. Campbell, S. C. Parker, D. E. Starr, *Science* **2002**, *298*, 811.

- [18] P. Pawlow, *Z. Phys. Chem.* **1909**, 65, 545.
[19] J. Dash, A. Rempel, J. Wettlaufer, *Rev. Mod. Phys.* **2006**, 78, 695.
[20] S. Magdassi, M. Grouchko, O. Berezin, A. Kamyshny, *ACS Nano* **2010**, 4, 1943.
[21] H. Van Swygenhoven, P. M. Derlet, A. G. Froseth, *Nat. Mater.* **2004**, 3, 399.
[22] T. Y. Hung, S. Y. Chiang, C. J. Huang, C. C. Lee, K. N. Chiang, *Microelectron. Reliab.* **2011**, 51, 1819.
[23] R. An, C. Wang, Y. Tian, H. Wu, *J. Electron. Mater.* **2008**, 37, 477.
[24] K. Subramanian, J. Lee, *J. Mater. Sci.: Mater. Electron.* **2004**, 15, 235.
[25] R. Hill, *Proc. Phys. Soc. Sect. A* **1952**, 65, 349.
[26] Y. Ding, C. Wang, L. Mingyu, B. Han-Sur, *Mater. Sci. Eng., A* **2004**, 384, 314.

Received: April 2, 2015
Revised: May 3, 2015
Published online: June 1, 2015